Spatial distribution of defects in a plastically deformed natural brown diamond

F.H.J. Laidlaw[a,b,*], P.L. Diggle[c], B.G. Breeze[a], M.W. Dale[c], D. Fisher[c], R. Beanland[a],

[a] Department of Physics, University of Warwick, Coventry, UK, CV4 7AL

[b] Centre for Doctoral Training in Diamond Science and Technology, Coventry, UK, CV4 7AL

[c] De Beers Group IGNITE™, Incubation Research, Maidenhead, UK, SL6 6JW

Abstract

Photoluminescence, Raman mapping, cathodoluminescence and transmission electron microscopy (TEM) have been carried out on a "zebra" diamond, containing both brown and colourless bands. The stone was cut into two and one part was given high-pressure high temperature (HPHT) treatment, removing the brown colouration. The parts were then cut into (110) sections. In the untreated stone the morphology of brown stripes is consistent with that of slip bands formed during plastic deformation and Raman mapping shows they are under strong compressive stress. Photoluminescence from N3 and H3 centres, as well as lines at 406.3 nm, 491.3 nm and 535.9 nm, are correlated with brown bands in the untreated sample, while cathodoluminescence shows that band-A luminescence is anticorrelated. HPHT treatment reduces internal stress, and eliminates or reduces correlated luminescence. TEM reveals long straight dislocations and dislocation dipoles in the brown bands, consistent with deformation by slip and concurrent intrinsic point defect production, while clear bands have curved and tangled dislocation networks. We postulate that vacancies produced by plastic deformation aggregate into clusters responsible both for the brown colouration and an increase in volume that results in compressive stress. The 535.9 nm line has characteristics of an interstitial-type defect and may be formed by the trapping of interstitials generated during plastic deformation.

Keywords

Plastic deformation, intrinsic point defects, correlative microscopy, natural diamond

* Corresponding Author, F.Laidlaw@warwick.ac.uk (Fraser Laidlaw)

1. Introduction

Plastic deformation is clearly linked to brown, pink, purple and violet colourations observed in diamond[1–3]. Of these colours, brown is the most commonly observed, with up to 98% of all mined diamonds containing some brown component to their colouration[4,5]. Colouration in plastically deformed type I diamonds tends to be localised within lamellae lying along {111} planes, while in type II diamond, the colouration is typically found with uniform distribution throughout the sample, although the occasional type IIa pink diamond does show some lamellae[5,6]. Single crystal natural stones, with brown lamellae separated by colourless regions are sometimes referred to as "zebra" diamonds. These coloured lamellae are consistent with slip bands in the material caused by plastic deformation[7], or deformation twins[2,8,9]. The appearance of coloured lamellae within colourless material is commonly referred to by gemmologists as "graining" (or specifically "brown-graining and pink-graining" in cases where the colouration is well defined)[2,5,9]. Brown colouration is a gradually increasing absorption towards shorter (blue) wavelengths[10], while pink colouration is caused by two absorption bands centred at 550 nm and 390 nm. Brown and pink colouration has been observed in both type I and II diamonds, suggesting no direct correlation with nitrogen content, while the lack of any sharp features in the absorption spectra of type IIa diamonds implies that an extended

defect is responsible for the absorption. The origin of pink colouration is currently unknown, but has been linked to twinning[2,9].

For ductile deformation of diamond to take place, temperatures > 900°C are generally required[11], although deformation can be induced at temperatures as low as 750°C with the use of soft indenters[12]. In nature, deformation is thought to occur during the diamond's residence in the mantle[13], where lithospheric diamonds can reside for up to 10^9 years while experiencing temperatures between 900 and 1400°C[14]. Plastic deformation can produce a variety of effects on the crystal that might in principle contribute to colouration of a diamond. The primary changes induced by plastic deformation are the generation and movement of dislocations within the material and/or the formation of deformation twins[2,5,9,15]. As deformation progresses, glide of dislocations causes slip bands to appear at the surface, while dislocations within the material rearrange themselves to reduce crystal stresses, leading to the formation of distinctive dislocation microstructures and causing work hardening of the material[7,16]. Owing to the link between the brown colouration and plastic deformation, dislocations were first suggested as a possible origin of the absorption[10]. However, not all dislocations were found to generate the necessary electronic states to produce absorption consistent with brown colour and the density of sites available to provide these states were found to be too low given the typical densities of dislocations[17] – of the order of 10^9 cm^{-2} . This indicates that some secondary effect is responsible.

Secondary effects of plastic deformation include the production of intrinsic point defects (both interstitials and vacancies) caused by the movement of jogged dislocations. Jogged dislocations are readily produced following the interaction of dislocations lying on two different glide planes[18]. The jogs have restricted mobility, pinning the dislocation in place, but can move non-conservatively by emitting point defects. Plastic deformation caused by an active glide system cutting through a pre-existing 'forest' of dislocations produces many jogged dislocations, and thus high concentrations of intrinsic point defects[17,19]. It has been demonstrated that dislocation densities of 10^9 cm^{-2} and a strain of 1% can produce 10^{17} – 10^{19} point defects cm^{-3} via this mechanism[19]. At the temperatures required for plastic deformation of diamond the equilibrium concentration of isolated point defects is very low, and they can readily migrate to form more stable complexes. For example, the H3 ($N\text{-}V\text{-}N^0$) centre, formed by the capture of a vacancy at an A-centre, is commonly observed at higher concentrations in areas showing evidence of deformation[20–22]. Another possible change induced by plastic deformation is the break-up of existing point defect complexes by moving dislocations, resulting in the creation of new point defects. For example, dislocation movement through A-centres has been proposed as the origin of a series of point defects, such as the "amber" centres and W7/N2 EPR centres, observed in plastically deformed diamonds[23,24].

The current consensus is that vacancy clusters are responsible for brown colouration, based on several observations[10]. Positron Annihilation Spectroscopy (PAS) suggests the presence of vacancy clusters, roughly spherical in shape and 30-60 vacancies in size, in brown diamond[25–27]. They are absent in colourless diamond, and their concentration decreases in the same way as brown colouration following high pressure high temperature (HPHT) treatment.[28] Combined optical excitation spectroscopy and PAS, along with DFT calculations, show that these vacancy clusters have an absorption spectrum that can account for the brown colour[29–33]. Dangling bonds from sp^2 bonded carbon on the inner walls of the cluster produce the necessary continuum of levels within the band gap. Vacancy cluster concentrations of 10^{15} cm^{-3} and monovacancy type defect concentrations of 10^{18} cm^{-3} have been measured in brown diamond by PAS[28], so plastic deformation can fully account for the point defect concentrations observed. Atomic resolution imaging of brown type IIa diamond has found interstitials absorbed onto the 90° partial dislocation, in both dissociated 60° dislocations and faulted dipoles, forming a prismatic dislocation loop. The preferential absorption of interstitials onto the dislocations over vacancies is a result of the dislocation bias[34], caused by the stronger interaction between the stress fields of the dislocations and the interstitials. Pink diamonds have more

complex behaviour and exhibit photochromism, with the pink colour bleaching to brown under UV excitation, reverting back to pink after heating or prolonged white light exposure. Charge transfer between multiple trap states may be the cause of the photochromism in pink diamond, with vacancy clusters likely to be one of these traps[6,35–37].

From the above, it is apparent that an improved understanding of the processes occurring during plastic deformation can assist in determining the origin of various point defects and deformation-induced coloration. In this regard, correlative microscopy is increasingly being used to obtain a more complete picture of the material properties and processes that have occurred, with the ability to image the sample on various length scales and extract more sample information than can be obtained from a single technique. In this paper we use photoluminescence (PL) and cathodoluminescence (CL) spectroscopy to detail the observed point defect distributions, 2D Raman mapping of crystal stresses, and Transmission Electron Microscopy (TEM) to understand the dislocation microstructure. We examine their relationship in a "zebra" diamond, containing both brown and colourless bands.

2. Methods and Materials

A banded brown type IIa stone was provided by De Beers, which was sectioned into two pieces. One piece was subject to HPHT treatment (2000 °C, 12 hours), while the other remained untreated. Subsequently, three thick plates were prepared from the two samples; two treated and one untreated plate, which were then thinned, by Element Six Ltd, down to 50 μm thickness. Offcuts from the untreated stone were retained for spectroscopic measurements. A summary of the plates is provided in Table 1. The plates measured 2 mm × 2 mm × 50 μm in size and the face of each plate was orientated close to the $[\bar{1}\bar{1}0]$ direction, with the square edges corresponding to <100> and <110> directions. Off-cuts were approximately 2 mm × 0.5 mm × 0.5 mm in size. The geographical origin of the original sample is unknown.

Table 1: Zebra diamond samples used in the study and their treatment.

Sample Name	**Treatment**	**Measurements**	**Size**
Plate A	2000 °C: 12 hours	Optical, PL, CL	2mm × 2mm × 50μm
Plate B	2000 °C: 12 hours	TEM, CL	2mm × 2mm × 50μm
Plate C	Untreated	TEM, CL	2mm × 2mm × 50μm
Sample D (offcuts)	Untreated	Optical, PL, CL	2mm × 0.5mm × 0.5mm

FTIR spectroscopy was attempted to map any A (N-N), B (N_4V) or B' (interstitial clusters) centres in the samples to assist in the interpretation of the PL maps, however the limited sample thickness caused interference effects which prevented meaningful spectra from being obtained. An FTIR spectrum of the complete rough stone found no evidence of A, B or C centres, indicating the sample is of type IIa, although inhomogeneities in defect concentrations throughout the stone may be present and the FTIR spectrum obtained may be unrepresentative of the prepared samples used here. It is also widely accepted that the sensitivity limit of FTIR in characterising nitrogen concentrations is 1 ppm, and so whilst the stone is classified as IIa, it is plausible a small amount of A or B centres are present especially given the presence of nitrogen-related defects in other spectroscopic measurements.

PL mapping was carried out on a Horiba LabRAM Evolution microscope and spectrometer using a 488 nm solid state laser, step size of 5 μm, and a Renishaw InVia confocal microscope using a 325 nm HeCd laser, step size of 7.5 μm, at liquid nitrogen (LN) temperatures. Raman mapping was carried

out on the Horiba LabRAM Evolution microscope and spectrometer using a 660 nm laser, step size 2 µm, at LN temperatures.

CL was carried out on a Zeiss Supra 55VP Field Emission Gun (FEG) SEM equipped with a Gatan MonoCL3 system. Samples were coated in a thin layer of carbon to neutralise sample charging. Panchromatic CL images were obtained using a Variable Pressure Secondary Electron (VPSE) detector, which allowed low-magnification images of the entire sample to be taken. In variable pressure mode, the VPSE detector detects photons emitted from gas in the chamber, ionised by secondary electrons emanating from the sample surface, whereas in high vacuum mode only photons generated by CL are detected. This use of the VPSE detector negates the need for a parabolic mirror, which only collects photons efficiently from its focal point. CL was carried out at temperatures of approx. -140 °C to increase luminescent intensity and line sharpness; imaging was carried out with an accelerating voltage of 5 kV, to maximise image resolution, while spectra were taken at 20 – 30 kV to maximise signal. This larger accelerating voltage produces a generation volume larger than that of imaging and the spectra obtained probes deeper into the sample.

The diamond plates B and C were thinned to electron transparency using Ar^+ ions in a Gatan Precision Ion Polishing System (PIPS). Continuous ion milling was carried out on one side at 5 kV with an incident angle of 5° for 3 hours, after which the sample was turned over and milled on the other side under the same conditions until a small hole was produced. This gave a large electron-transparent area, with thicknesses of < 100 nm being achieved near the edge of the hole and < 200 nm up to 1-2 µm away. Final polishing of both sides of the specimen, at voltages between 0.5 - 3.5 kV and at angles of 3 - 3.5°, was carried out to ensure a clean and flat surface. Conventional TEM imaging was carried out using a LaB_6 JEOL 2100 Plus HC using an accelerating voltage of 80 and 200 kV. Bright Field (BF), Dark Field (DF) and Weak Beam Dark Field (WBDF) imaging was carried out using a 220 diffraction condition.

3. Results

3.1 Optical Imaging *of Sample D (untreated)*

Optical images of the untreated sample, Sample D, show the brown colouration is concentrated in distinct bands, Figure 1(a). The sample has been cut and polished with the major face aligned to (110). The brown bands are orientated at approx. 54° (± 3°) to the (001) face, consistent with the intersection of a $(\bar{1}11)$ plane on the (110) face, as expected for slip bands. We investigate the right-hand side of the sample in detail and to allow spatial correlation it is helpful to recognise the dark and narrow band marked ■ in Fig. 1(a). Birefringence imaging, sensitive to shear strain in the material that induces optical anisotropy, is shown in Figure 1(b). This clearly shows the bands and the highly strained nature of the diamond. The strain appears to vary across the sample, with a distinct banding pattern, where broader bands in the material show a higher order of birefringence at the interfaces.

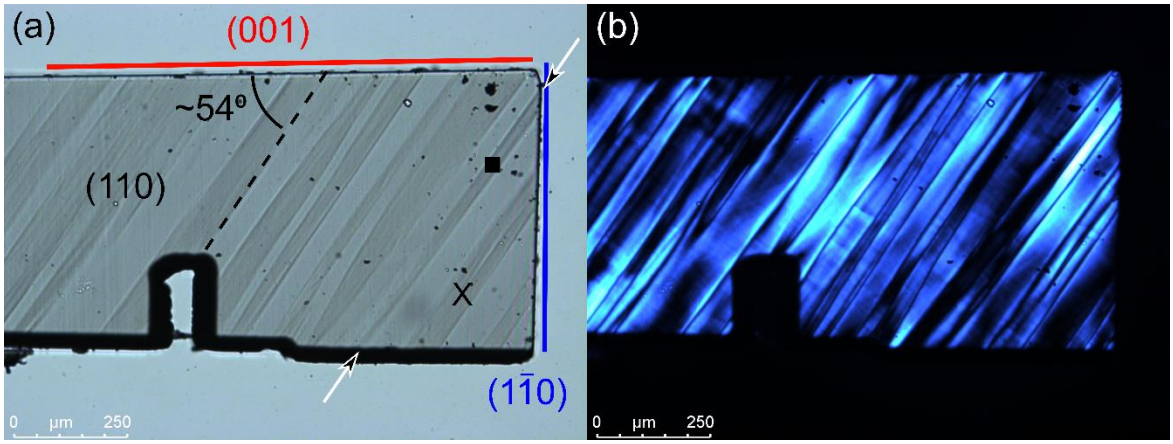

Figure 1: (a) Optical Image of section of Sample D (untreated sample). Brown colouration appears as bands running from bottom-left to top-right. (001) and $(\bar{1}10)$ planes highlighted by red and blue respectively. X marks approximate location of PL spectra of Figure 3. ■ marks a distinct brown band that is a useful reference point. (b) Imaged with cross polarisers to show birefringence. Brighter material is highly strained.

While birefringence images show shear strain, the first order Raman line can be used to measure hydrostatic stress, calculated from the shift Δ in the 1332.5 cm^{-1} position in unstrained diamond, using $\sigma = \Delta/\alpha$, where α is the hydrostatic stress gauge factor (approx. 2.9 cm^{-1}/GPa)[38]. Each spectra is fitted with a single pseudovoigt line shape, and the resulting maps of the Raman shift and stress are shown in Figure 2, as well as the line width. Broadening of the Raman line indicates the presence of different hydrostatic stresses in the excitation volume, i.e. the presence of stress gradients, point defects or dislocations. We note that despite mounting the sample normal to the objective, the area under the Raman peak fit varies across the bands which can be found in Figure S1.

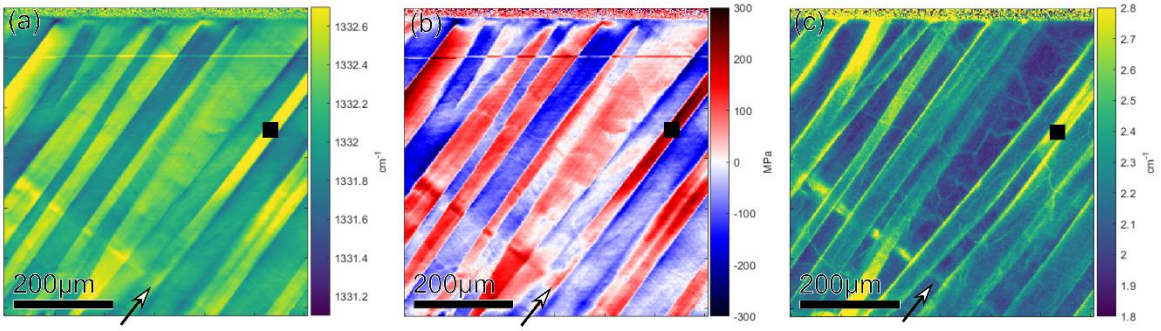

Figure 2: Raman maps using 660 nm laser excitation of Sample D (untreated sample, right side of Figure 1). (a) peak position; b) hydrostatic stress; (c) peak width. Brown bands are in compression and colourless bands in tension. ■ highlights the same sharp brown band shown in Figure 1.

Comparing the map of hydrostatic stress, Figure 2(b), with Figure 1(a) it is seen that brown bands are in compressive stress, particularly the dark brown band ■, while colourless bands are under tension. Stresses approaching 300 MPa can be found adjacent to interfaces between bands, with lower stresses near the middle of the bands. The interfaces themselves tend to coincide with the plane of zero stress that must be present between regions in compression and tension, although the stress gradient is high as evidenced by an increased width of the Raman line, Figure 2(c). Also visible in Figure 2(c) is a cellular network of dislocations. The broadening of the Raman line is consistent with the high stress gradients produced by a high density of dislocations. Manual inspection of the fits show the Raman line is well characterised by the single pseudovoigt function, indicating the internal stresses are not high enough to remove the triple degeneracy of the first order Raman[39]. This network has no correlation with the colouration and in fact cuts across both colourless and brown bands in many places. This cellular network may have played the role of forest dislocations[19] for subsequent plastic deformation that gave rise to the brown colouration.

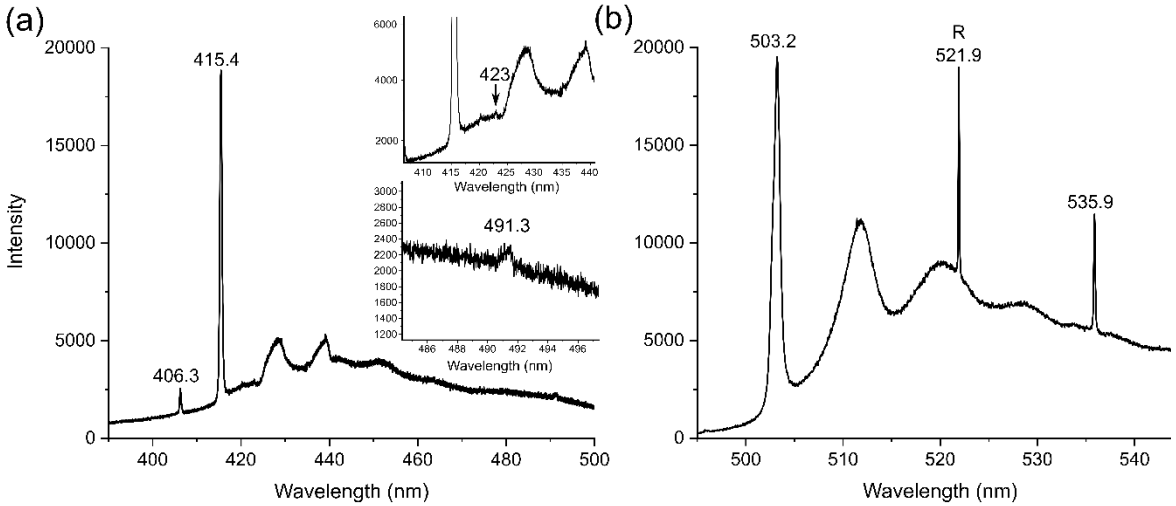

Figure 3: PL spectra from a brown band in untreated material (sample D) as indicated in Fig. 1a. (a) in the range 390 – 500 nm. Zero-phonon lines (ZPL) can be seen at 406.3 nm and 415.4 nm (N3). Spectrum obtained using 325 nm laser excitation at LN2 temperatures. Inset, small features between N3 phonon sidebands and small peak at 491.3 nm. (b) PL spectrum in the range 495 – 545 nm. Raman line (R) observed at 521.9 nm. ZPL observed at 503.2 nm (H3) and 535 nm. Spectrum obtained using 488 nm laser at LN temperatures.

PL spectroscopy in the centre of a brown band (position marked in Figure 1) indicates the presence of several point defects, Figure 3. As expected for plastically deformed natural diamond, the nitrogen-related zero-phonon line (ZPL) of both N3 (415.4nm) and H3 (503.2nm) are present, with phonon sidebands at 428, 438 and 512, 520, 528 nm respectively. In addition to the N3 and H3 lines, the first order Raman line is present at 521 nm and a strong line can be seen at 535.9 nm whose origin is unknown. Weak lines can also be observed at 406.3 nm and 491.3 nm, and even finer features are present between the sidebands of the N3 centre at 423 nm, Figure 3(a) inset, although the intensity of these features is low and accurate determination of peak wavelength is difficult. Mapping of these defects was not possible due to their weak signal. In order to further understand the origin of PL features, we performed mapping of the N3, H3 and 535 nm luminescence over the same region as shown in Figs. 1 and 2, the results of which are shown in Figure 4. Fitting of the N3, H3 and 535.9 nm lines was carried out with a single pseudovoigt peak. Deconvolving the ZPL of the H3 defect by fitting two pseudovoigts was attempted, and the results can be seen in the Supplementary Information, Figure S3.

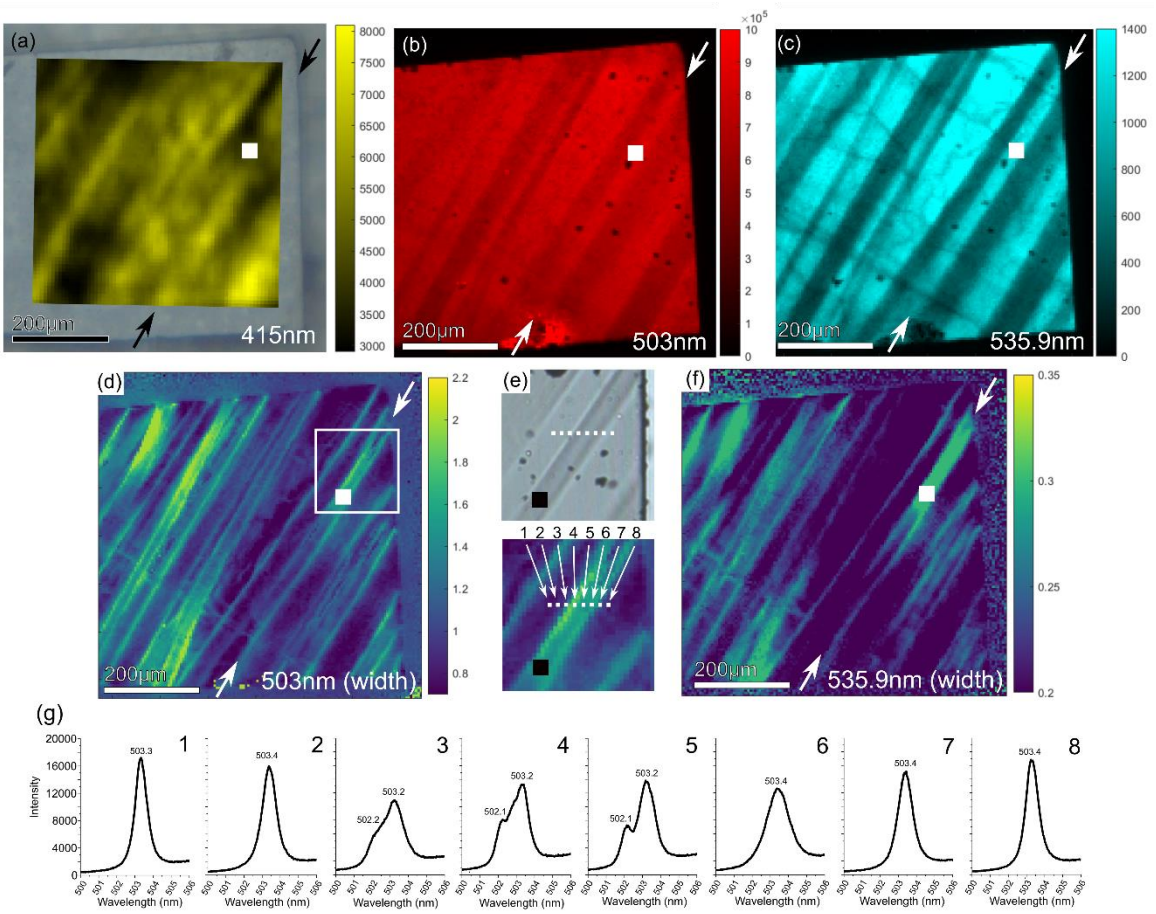

Figure 4: PL maps of untreated material (sample D). (a) N3(415.4 nm) peak intensity, (b) H3 integrated intensity (500 – 506 nm) and (c) 535.9 nm line intensity. (d) Map of H3 line width, (e) Region shown in (e) with numbered pixels across band interface. (f) Map of 535.9nm line width. (g) H3 line at numbered pixels in (e) showing the splitting of the peak across the band interface. Increased intensity represents a broader peak. Black spots in (b, c) are foreign particles on the surface. Defect lines are unnormalized with respect to the Raman line, see discussion. Arrows highlight the band ■.

The distributions of all three strong luminescence centres are correlated with colouration. The N3 intensity is the least correlated; brown bands appear to have stronger N3 luminescence in general but the banded N3 structure only vaguely resembles the stripes of colouration in Fig. 1(a). There are bright and dark patches that are unrelated to the bands and the latter may be due to quenching from the cellular dislocation network. The diffuse appearance is partly due to the relatively large step size of the scanning laser beam (of 7.5 µm) and the use of interpolation. The H3 intensity map is integrated over the spectral window of 500 – 506 nm. The fitting of the H3 line is complicated by the splitting of this peak, as shown in the SI, but broadly agrees with the integrated window. The intensity of H3 is ~25% higher in brown vs colourless bands while the 535 nm luminescence shows much higher contrast, typically doubled in brown bands. Quenching of the 535 nm line by the cellular dislocation network is clearly visible, while dislocations hardly affect the H3 map. Both H3 and 535 nm lines show broadening that matches the stresses observed in the Raman map (Figures 4(d) and 4(f)). Further investigation reveals that the broadening at brown/colourless boundaries is seen as splitting of the peak into two as shown in Figure 4(e) and (g). This indicates that the energy of these defects is affected by the stress gradient at these interfacial regions.

In summary for these observations, brown bands have a higher content of H3 and N3 centres, associated with nitrogen-vacancy complexes, and an unknown complex luminescing at 535 nm. However, the correlation is low for the H3 centre and N3 is only slightly enhanced in brown bands.

Both H3 and 535 nm show broadening/splitting near to boundaries indicating a sensitivity to stress and/or strain, but quenching of luminescence by high dislocation densities in the cellular dislocation network only affects the 535 nm and N3 lines.

3.2 Optical Imaging *of Plate A (treated)*

Optical imaging of the treated stone, Plate A, shows a marked reduction in the brown colouration, Figure 5, although faint bands can still be seen. Birefringence imaging, Figure 5 (b), shows that shear strain remains present in the sample, but has become more restricted to interfaces between the colourless and formerly brown bands.

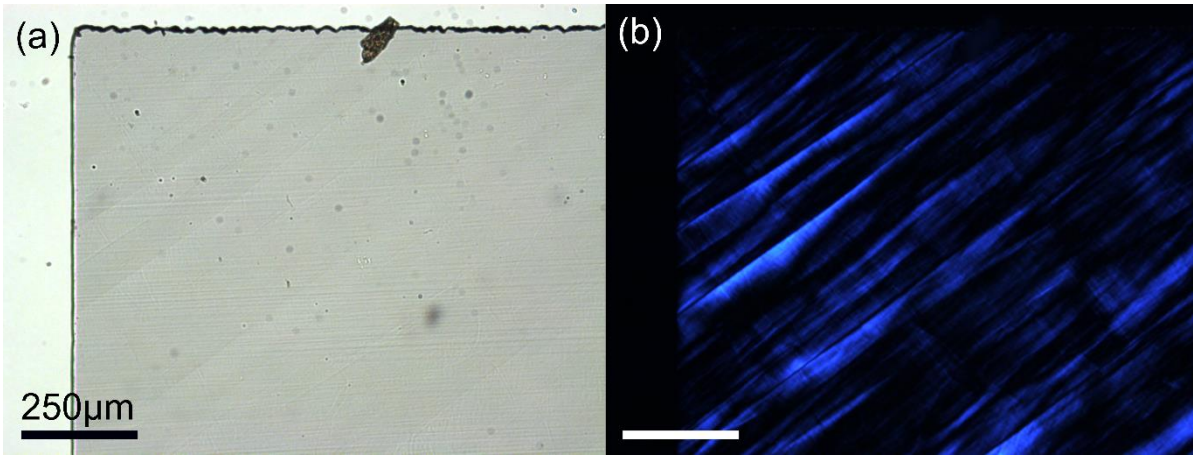

Figure 5: (a) Optical image of Plate A (HPHT treated) stone. Banding can still be observed although the colouration is substantially reduced. (b) Birefringence image showing some strained regions remain after treatment.

Raman mapping confirms that substantial internal stresses are still present in the sample, as shown in Figure 6 (note this is area does not correspond to that of Figure 5, although it is in the same orientation). Plotted at the same magnitude as Figure 2, it is clear to see a reduction in contrast, indicative of a reduction in stress magnitudes. A histogram of stress values from the maps is provided in the supplementary information, Figure S2, which confirms a reduction in the magnitudes and spread of stresses measured. The standard deviation of stress values have dropped from 92 MPa, in the untreated stone, to 52 MPa, in the HPHT treated stone. Stress gradients, as inferred by the width of the Raman line (Figure 6c), still exist at interfaces between bands but are now equivalent to, or only slightly larger than, those at cellular dislocation networks. Away from the network of defects, stress gradients within the bands are low, producing less than 2 cm^{-1} of broadening of the Raman line.

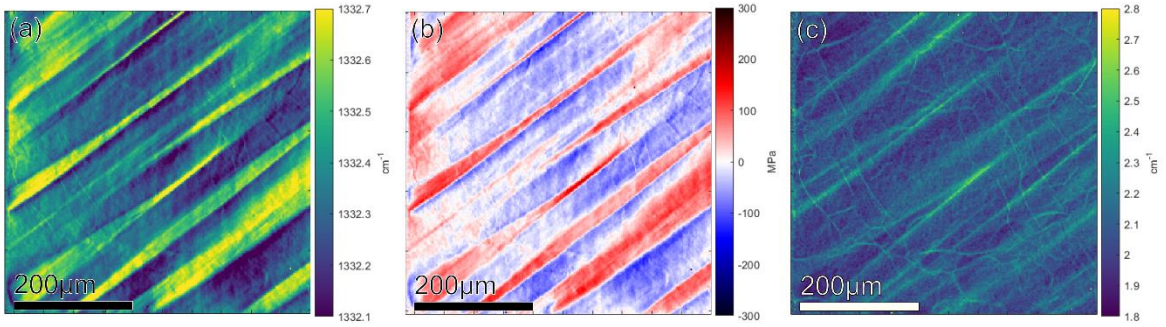

Figure 6: (a) Map of Raman peak position in HPHT treated Plate A, (N.B. different area from Figure 5a). (b) Map of hydrostatic stress calculated from shift in Raman peak position. (c) Map of Raman peak width.

We also observe that PL spectra are changed significantly by HPHT treatment. Spectra from a region that has lost its brown colouration is shown in Figure 7. The 406.3 nm, 491 nm and 535.9 nm lines have been completely removed following HPHT treatment. By comparing the H3 (503.2 nm) and N3 (415.5 nm) ZPL intensities to the first order Raman intensity, we also qualitatively observed a reduced intensity when compared to the untreated sample. Maps of the H3 and N3 ZPL intensities can be seen in Figure 8.

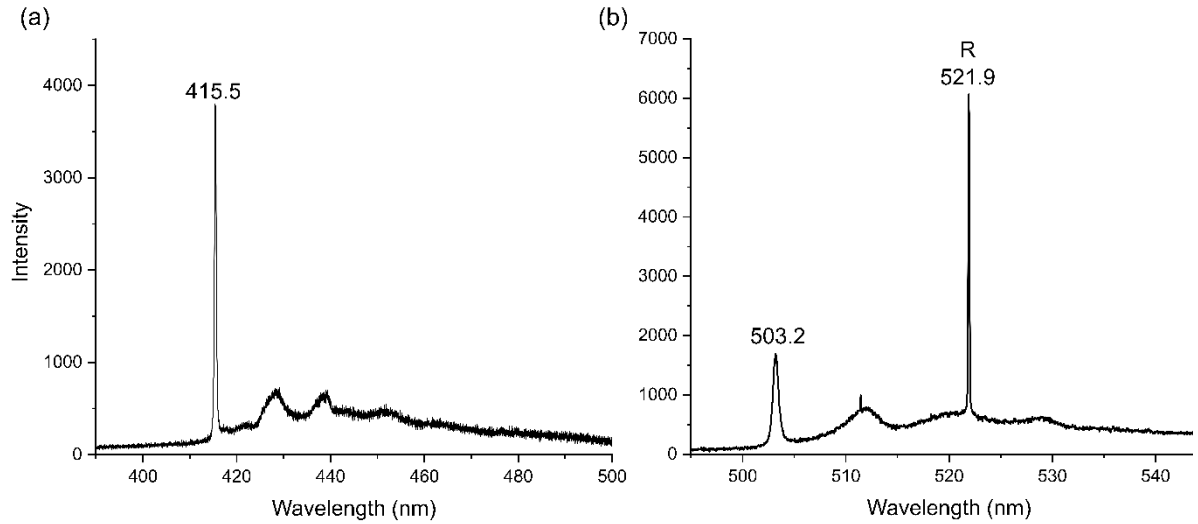

Figure 7: (a) PL spectrum in the region 390 – 500 nm from a previously brown region in HPHT treated Plate A. The ZPL at 406 nm and 491 nm are absent post HPHT treatment. Spectrum obtained using 325 nm laser at LN temp. (b) PL spectrum in the region 495 – 545 nm. A Raman line is observed at 521 nm. The H3 ZPL line (503.2 nm) is still present but at lower intensity, while the 535 nm line is completely removed. Spectrum obtained using 488 nm laser at LN temp. PL spectra are representative of entire mapped area.

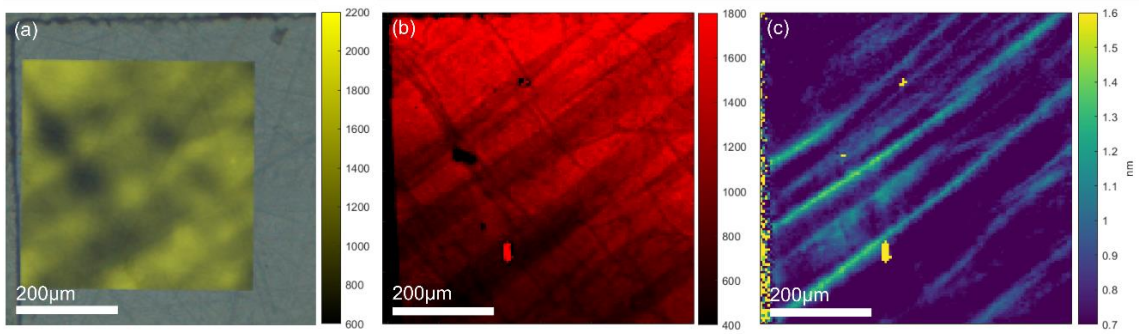

Figure 8: PL maps of HPHT treated material (sample A). (a) N3 (415.5 nm) and (b) H3 (503.2 nm) peak intensity maps. N3 concentrations appear to be larger in areas containing fewer H3 centres. (c) Map of the H3 line width.

As seen previously in the untreated sample, the distribution of the N3 centre is patchy and while a correlation with the banded structure is evident (again, N3 is generally higher in the formerly brown bands) the correlation is not as strong as that of the H3 centre, as can be seen in Figures 8 (a) and (b). The H3 centre also remains stronger in the formerly brown bands, and is still significant in colourless material. Both H3 and N3 show strong quenching at cellular dislocation networks. No splitting of the H3 peak is observed and the width is smaller than in the untreated sample with a maximum FWHM of 1.6 nm in Figure 8(c) in comparison with 2.2 nm in Figure 4(d), consistent with the lower internal stress and strain observed in the Raman map and birefringence image.

These results indicate a significant reduction in the density of point defect complexes that accompanies the loss of brown colouration with HPHT treatment, as well as lower internal stresses and strains.

3.3 Cathodoluminescence (CL)

Cathodoluminescence images provide a link between PL maps and TEM images as they give similar information to PL but at a resolution limited mainly by the diffusion length of the non-equilibrium charge carriers generated in the material by the primary electron beam. Panchromatic CL images of Sample D and Plate A are shown in Figure 9. The banded structure is readily visible for both the untreated and treated samples, although in these panchromatic CL images brown, and formerly brown, bands have reduced CL intensity whereas in the monochromatic PL maps of Figures 4 and 8 they have higher H3, N3 and 535 nm line intensities, that is, contrast appears reversed. Quenching of luminescence by the cellular dislocation network, which matches that in PL maps, is also visible. The contrast between the bands in the panchromatic CL images is due to higher intensity of band A emission (~400-500 nm) in the colourless bands, as can be seen in the CL spectra of Figure 10. These spectra were normalised to be equal at background levels (an emission wavelength of 300 nm) to allow quantitative comparison. In the untreated stone the luminescence appears uniform across the brown bands while that from colourless bands is patchy. Some interfaces between the bands have enhanced luminescence. The difference in Band A emission between colourless and formerly brown bands is smaller, but still readily observable after HPHT treatment (Figure 10(b)). However in the HPHT treated sample, the lower luminescence is more strongly affected by non-radiative recombination at dislocations and is patchy and variable (Figure 9(b)).

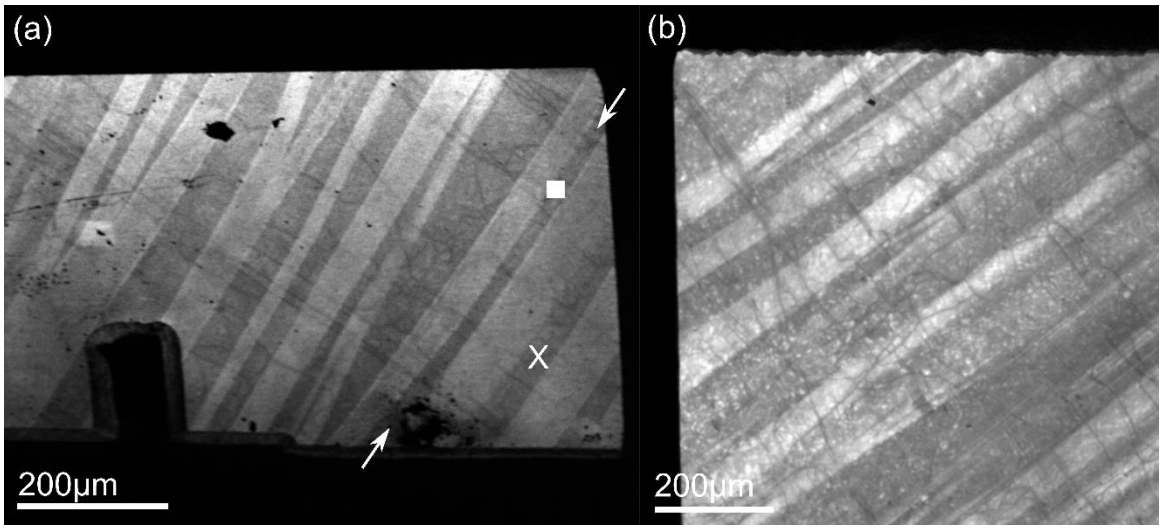

Figure 9: Panchromatic CL images obtained using the VPSE detector of (a) Sample D - untreated diamond and (b) Plate A – HPHT treated diamond. Brown bands exhibit less luminescence than colourless bands. References ■ and X in (a) link these to Figures 1, 2 and 4.

In the CL spectra of both samples, Figure 10, the N3 ZPL (415 nm) and its phonon sidebands can be seen on top of Band A emission for both brown and colourless bands. Additional peaks are seen in the untreated sample, with lines at 491 nm, 503 nm and 536 nm. The 406 nm line in the untreated sample observed by PL is not observed in the CL spectrum and other strong PL lines, H3 (503 nm) and 535 nm lines are weak. Conversely, the 491 nm line is much stronger in CL compared to PL.

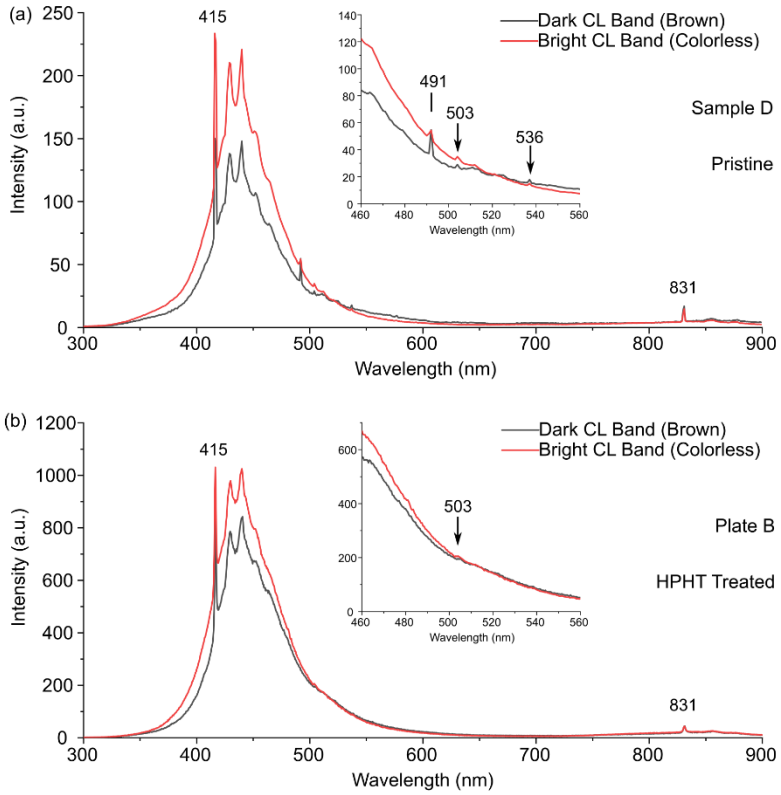

Figure 10: CL spectra of (a) Sample D (untreated) and (b) Plate B (HPHT treated) at LN temperature (Normalised at 300 nm). Spectra reveal the presence of the N3 defect at 415 nm, overlaid on the broad peak of band A emission in both untreated and treated sample. Second order N3 ZPL can be seen at 831 nm. Untreated sample shows additional peaks at 491, 503 and 536 nm in agreement with PL spectra. A small H3 peak is observed after treatment.

3.4 T*ransmission Electron Microscopy (TEM)*

Panchromatic CL imaging was used to locate a boundary between a brown and colourless band in Plate C after thinning to electron transparency, shown in Figure S4. TEM imaging was then carried out across this boundary. The images shown in Figures 11(a, b, c and d) use a $\mathbf{g}3\mathbf{g}$ $2\bar{2}0$ weak beam dark field (WBDF) imaging condition, in which dislocations appear as bright lines on a dark background; part of the cellular network of low angle grain boundaries identified by CL (Figure S4) is highlighted in yellow in the TEM image (Figure 11 (a)) to show their relationship. Clear differences in the dislocation microstructure of the two bands can be seen, Figure 11(a). In brown material (Figure 11(b, c)) large numbers of long, straight dislocations and dislocation dipoles can be observed, all with line directions parallel to the axis of the band, i.e. on the $(\bar{1}11)$ plane. In the colourless band, (Figure 11(d)) dislocations form a tangled three-dimensional network with many interactions and curved segments. Due to complexity of these networks the dislocation density is difficult to estimate, but there is no obvious large difference in dislocation density in the two bands, only the way they are structured.

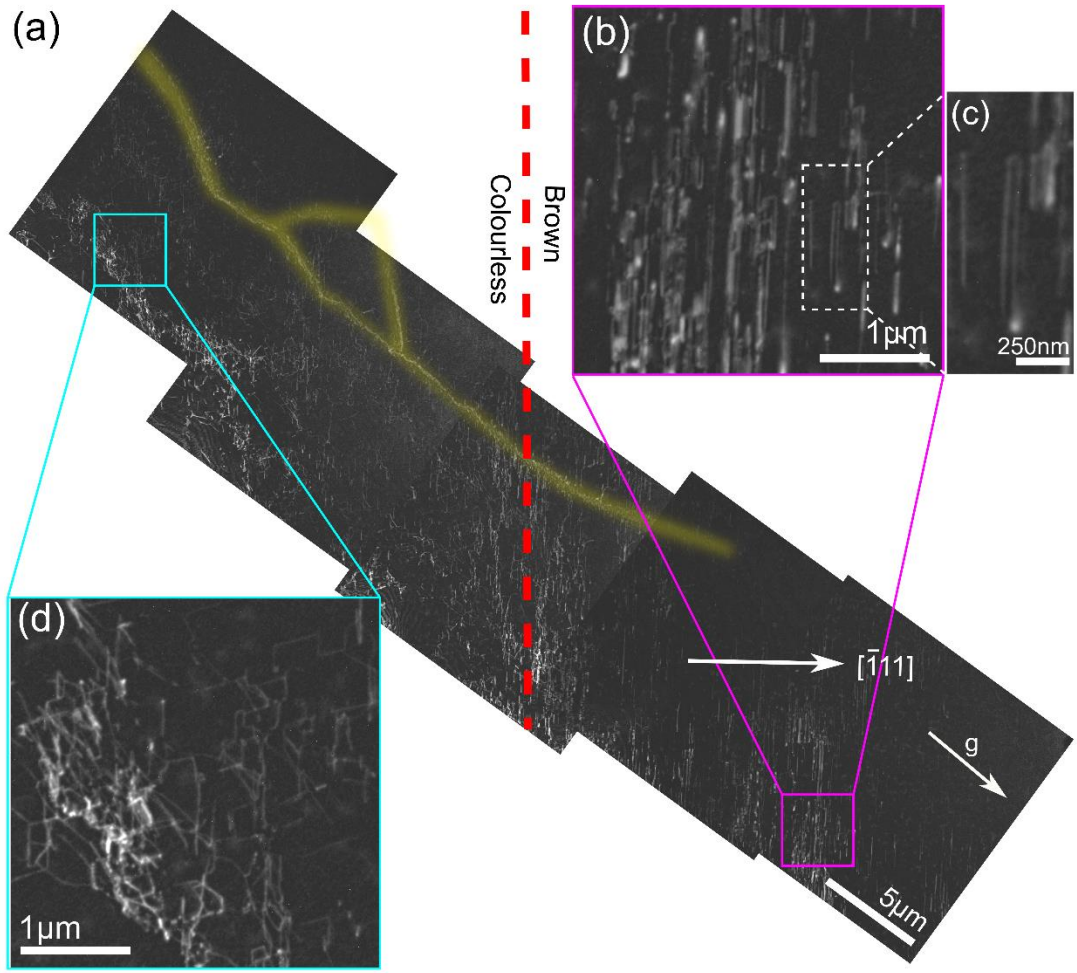

Figure 11: (a) WBDF **g**3**g** 2$\bar{2}$0 TEM image of dislocation microstructure across the boundary between a brown and colourless band in untreated diamond (Plate C), approximate location highlighted by red dashed line. Boxes highlight areas of (b) and (d). Distinctive dislocation network identified by CL is highlighted in yellow. (b) Dislocation microstructure within the brown band showing the are predominantly straight parallel dislocations and dipoles. (c) Cropped image of area highlighted in (b) showing a dislocation dipole. (d) Dislocation microstructure within the colourless band showing a tangled dislocation network.

Higher magnification images of dislocation dipoles in the brown band are shown in Figure 12. Figure 12(a) is again a WBDF image in which dislocations appear as bright lines. A high density of long straight dislocations can be seen lying parallel to the axis of the band, on ($\bar{1}$11) planes, running bottom left to top right, as well as dislocations cutting through their glide plane, running roughly horizontally with rather variable line directions in the plane of the TEM specimen, between [$\bar{1}$10] and [$\bar{2}$21]. These dislocations are not glissile and their variable line direction indicates that they are either formed during growth of the crystal or have undergone some climb; in either case they precede the arrival of the straight glissile dislocations[40–43]. Figures 12(b) and (c) show the interaction in more detail with a pair of bright field TEM images with opposite **g**-vectors. The reversal of contrast in these images show that many of the straight defects are dipoles. This contrast reversal is marked by black and white bars for a particularly widely-spaced dipole in Figures 12(b) and (c) but can also be seen for other defects.

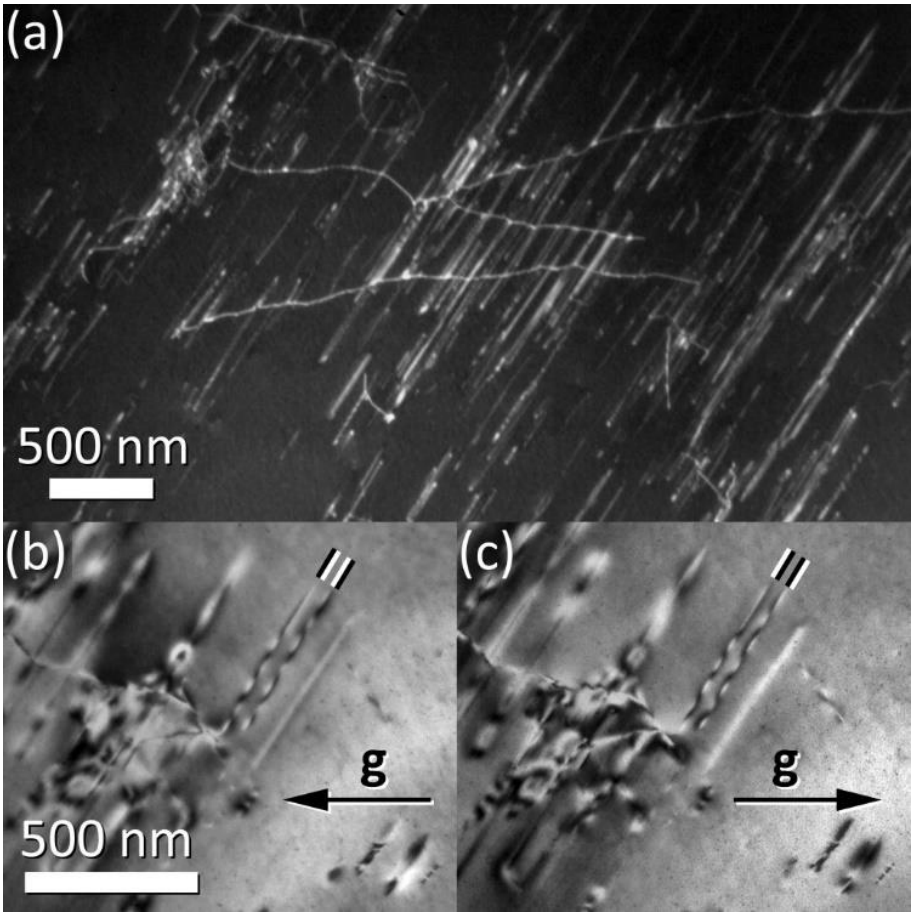

Figure 12: Dislocations and dislocation dipoles in a brown band in untreated diamond (Plate C). (a) WBDF TEM image of forest dislocations (roughly horizontal) that have interacted with dislocations gliding on the (111) plane, which are straight and run top right to bottom.(b) and (c) A pair of BF TEM images with reversed **g**-vector. For dipoles, contrast changes from inside to outside, indicated by the black and white bands for one dipole with a wide spacing (~30nm) between the dislocations.

After HPHT treatment the general dislocation structure appears unchanged as shown in Figure 13. Dislocation dipoles remain in the formerly brown bands and dislocations are still observed in tangles in the colourless band. Since it is not possible to examine any given structure before and after HPHT treatment, changes in individual dislocation configurations cannot be determined.

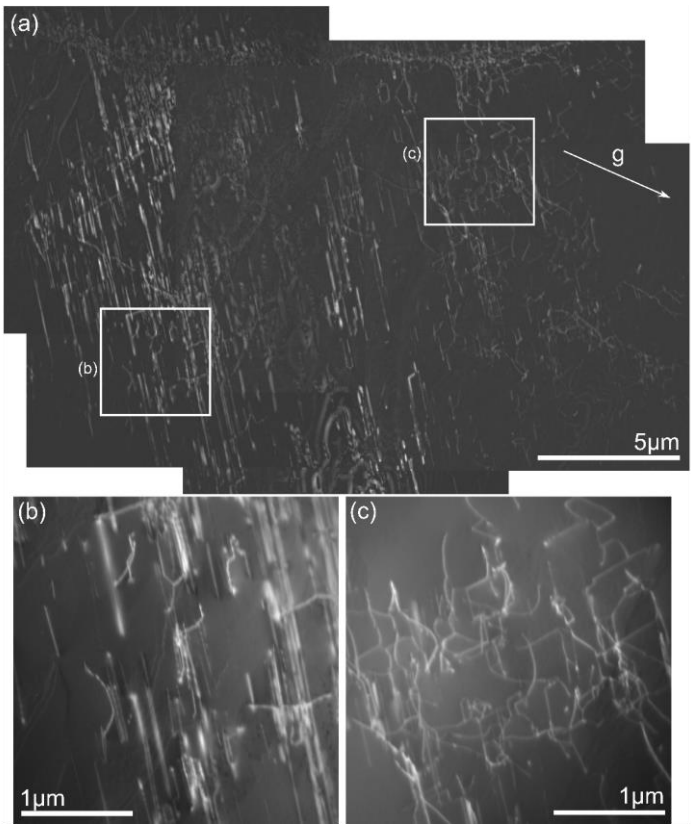

Figure 13: DF TEM image of dislocation microstructure in HPHT treated diamond (Plate B) across the boundary between a formerly brown band (left) and a colourless band (right). White boxes highlight areas of (b) and (c). (b) Higher magnification image of dislocation structures in the formerly brown band. (c) Higher magnification image of dislocation structures in the colourless band.

4. **Discussion**

The optically-active defect distributions observed in this zebra diamond are strongly affected by the plastic deformation it has experienced, which is evident in its physical microstructure. Colourless bands extend across the whole crystal, while brown bands tend to be wedge-shaped and can terminate at a sharp point to bifurcate colourless material. No twins are observed. The microstructure is consistent with a ductile fcc material that is well into stage II deformation[44], where the majority of plastic deformation has taken place in lamellae (slip bands, i.e. the brown bands), with boundaries that characteristically lie close to a {111} plane[7,45]. This notion is backed up by the dislocation microstructure; those in colourless material are tangled and curved and it is unclear if they are at all mobile, while in brown material high densities of straight dislocation dipoles are present, which can only have been produced by glide of many dislocations interacting with forest dislocations. The dipoles are primary evidence for the production of high densities of point defects by plastic deformation[40], and are formed when a glissile dislocation passes around several forest dislocations that cut through its glide plane, process shown in Figure 14.

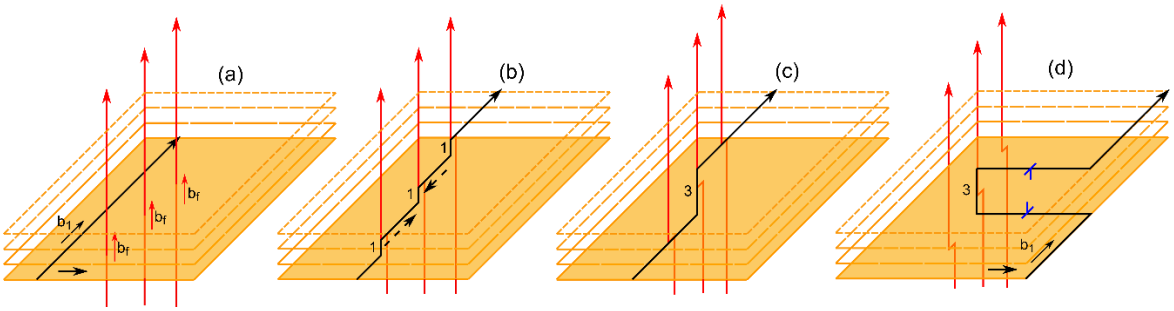

Figure 14: Formation of dislocation dipoles by the movement of a screw dislocation through a forest of screw dislocations. (a) A screw dislocation with Burgers vector b_1 moves to the right approaching three forest screw dislocations with Burgers vector b_f. (b) Each forest dislocation creates a unitary jog on dislocation b_1, likewise dislocation b_1 creates jogs in each forest dislocation. (c) Unitary jogs have combined to form a jog with height of three glide planes. (d) Dislocation b_1 continues to move to the right, pulling out a dislocation dipole with height of three glide planes from the immobile jog. (N.B. Height of dipole is for illustration of the mechanism and should not be taken to imply the stability of a dipole with a height of three glide planes.

For each forest dislocation with a screw component, the dislocation is displaced by a lattice translation vector, increasing the separation between the two arms and creating a dipole. For dipole separation above a critical height (h_c) the attractive force between the dislocations is insufficient to cause their annihilation and they remain stable in the crystal. These remnant dipoles can be observed in Figures 11, 12 and 13. Dipoles with separation below h_c annihilate, releasing interstitials or vacancies as they do so. (Which point defect is produced depends simply upon the sense of the displacement of the dislocations forming the dipole. Estimates suggest that both interstitials and vacancies are produced in roughly equal numbers.[19]) The value of h_c is not known precisely, but is estimated to be a few monolayers; previous studies have found dipoles with separations as small as 12 monolayers[19,46]. Although annihilated dipoles no longer exist to be seen in TEM images, the presence of larger dipoles indicates that the mechanism has been active. The point defects so produced easily migrate at the high temperatures required for plastic deformation[11,14,47] and since their equilibrium concentration is very low[19] they aggregate into clusters or are absorbed at sinks such as dislocations. Some point defects may also be released in the initial stages of dislocation glide in slip bands, by the disturbance and break up pre-existing point defect complexes. The point defect concentration generated by plastic deformation is large enough to account for all vacancy clusters observed in brown diamond[19]. The high flux of point defects, as they diffuse through the material before finding a stable location, is also likely to both change existing point defect complexes containing impurities such as nitrogen (e.g. by capture of a vacancy V) or enhanced diffusion[47,48].

These microstructural changes have a strong impact on the luminescence properties of the stone and are evident in the PL and CL spectra of the stone before HPHT treatment. Even though this is nominally a type IIa diamond, with no detectable nitrogen signature in FTIR spectra from the rough stone, PL spectra from brown bands in the untreated sample are dominated by the zero-phonon line of N3 (N_3V, 415.4nm) and H3 (usually ascribed to a N-V-N^0 defect[49], 503.2nm) as well as the first order Raman line at 521.9 nm and a line at 535.9 nm. Weaker PL lines at 406.3 nm and 491.3 nm are also seen in brown stripes of the untreated sample. Generation of point defects produces a volume expansion of the material[50,51] and the compressive stress observed using the Raman line in Figs. 2 and 6 is thus evidence of point defect production in brown bands. The amplitude of the Raman line also changes between the brown and colourless bands (Figure S2). Typically, PL lines are ratioed with respect to the Raman line, as an internal normalisation, removing the influence of laser power and the effect of fluctuations from the system[52,53]. Due to the variation in Raman amplitude, which appear to be from the sample itself rather than the instrumentation, normalisation of PL lines with respect to the Raman line was not carried out. Despite mounting the sample perfectly flat relative to the microscope objective, it is not understood why the Raman amplitude changes by correlation of the

brown and colourless bands, and so this requires further investigation to understand the underlying principles of Raman emission.

In the untreated sample, N3 PL maps show some correlation with the brown bands while the H3 and 535.9 nm maps have a perfect correspondence. All have higher concentration in brown bands with reduced intensity at dense dislocation networks for the N3 and 535.9 nm lines. It has been suggested that plastic deformation can break-up B-centres (N_4V), thus increasing the concentration of H3, N3 and single N defects[54]. No line is observed at 496 nm in these samples that would correspond to the H4 centre, a defect comprised of 4 nitrogen atoms and 2 vacancies (B-centre + V; N_4V_2) [55] and here implied as a PL proxy for the B-centre. Whilst the H4 centre is not thermally stable above 1400°C[49] it is also said to be correlated with a line at 490.7 nm which itself is linked to plastic deformation[52]. Conversely, the annealing behaviour of the 490.7 nm line does not follow that of H4, with it annealing out at higher temperatures[56,57]. As will be discussed, we do observe a line at 491.3 nm which has some correlation to the brown bands in this material, but it is not clear whether this is the same defect as the 490.7 nm line. When considering all of this with the type IIa nature of the samples studied here, it is uncertain if any B-centres formed during growth and have then subsequently broken up (due to moving dislocations) in order to form the N3 defects observed. Ultimately then, we are unable to deduce which mechanism of N3 formation is favoured with these type IIa research samples. The route is likely convoluted with multiple mechanisms such as the generation of vacancies by plastic deformation and their subsequent capture by nitrogen defects[18–20,48], interstitial assisted aggregation[48,58], plastic deformation related enhanced nitrogen aggregation[8], and any potential B-centre breakdown[54]. To unravel this further, additional correlative microscopy and spectral mapping on type Ia material should be considered.

The H3 line is sometimes present as two peaks. Whilst the deconvolution of the H3 peak is difficult to apply robustly within this dataset, individual spectra in Figure 4(g) show that splitting is strongest at the transition from brown to colourless. Davies et al.[35] showed that the H3 line splits under the application of uniaxial stress and the maximum separation observed here of 5 meV suggests a stress between 200 and 600 MPa, consistent with the rapidly changing Raman shift at these locations. Alternatively, the second peak could be the 3H defect, (ZPL 503.5 nm), associated with self-interstitials[59]. The 3H defect is stable up to temperatures of 800 °C so could conceivably remain stable during plastic deformation at relatively low temperatures[60]. However, since deformation at temperatures above 1000 °C is more typical, and stress gradients are clearly present, the stress-splitting hypothesis is stronger. Davies et al.[35] also showed that stress reduces H3 line intensity, but the observed difference (~25%) between brown and colourless bands would requires stresses >2.5 GPa. The contrast is thus probably a consequence of the low nitrogen concentration in combination with vacancy production in the brown bands, which would allow almost complete conversion of N-N to N-V-N at relatively low vacancy concentrations even in colourless material.

The 535.9 nm line observed here has the strongest intensity variation from brown to colourless bands and is probably the same as the line at 535.8 nm commonly observed in Argyle diamonds and some brown diamonds. The origin of this emission is unknown. It has been observed around inclusions and deformation lamellae in milky type IaB diamonds suggesting it is a product of plastic deformation,[55] possibly related to the presence of B-centres and other related defects[2,57,61]. Gu and Wang[55] found it to be correlated with the H4 line (which, as noted above, is absent in this stone). Uniaxial stress measurements of the 535.8 nm defect indicate it has monoclinic I symmetry and movements of the line in response to stresses are small meaning this defect is unlikely to contain a vacancy[62]. Thus, the results shown here, and previous studies, suggest the origin is due to point defects – in this case self-interstitials, rather than vacancies – and this is again consistent with their formation by plastic deformation. Figure 4(c) shows this line is either quenched, or not present, at the cellular dislocation network suggesting that the interstitials are captured by dislocations as seen in our previous work[19].

The weak 406.3 nm and 491.3 nm lines seen in brown bands here match those seen by Nadolinny et al.[63], who observed lines at 406, 491 and 423 nm (the latter also seen in this stone but extremely weak). They correlated these signals with an EPR signal from dangling bonds in the core of dislocations[63]. Other observations associate them with nitrogen in brown diamond,[49] and Graham and Buseck proposed that their 491.3 nm line was caused by the movement of a dislocation through an A-centre, forming a N-C-C-N defect[64]. Another study in agreement is that of Collins & Woods who observed a strong 490.7 nm line using CL spectroscopy in brown type Ia diamond, again accompanied by a 423 nm line and correlated with slip bands [57,65]. Gaillou et al.[2] observed a ZPL at 405.5 nm, proposed to be a strain-modified N3 centre, that may be the same as the 406.3 nm observed here. However, the accompanying line at 491 nm that we observe was absent, which could simply be because it is very weak, but could indicate that the 405.5 nm defect is a different entity. Here, phonon sidebands are obscured by the N3 ZPL and accompanying structures, so a good comparison cannot be made. Nevertheless, these prior observations and our results indicate that the 406.3, 491.3 and 423 nm lines are due to nitrogen-containing defects, formed or modified by plastic deformation or dislocation strain fields.

In CL spectra from the untreated stone the N3 line and its phonon sidebands are strong and clearly visible. The H3 and 536 nm lines are also present in brown bands, but very weak, while the 491 nm line is significantly stronger, illustrating the different selection rules for luminescence from optical excitation (PL) and carrier recombination (CL). However, the spectrum is dominated between 400 and 500 nm by band-A luminescence. The origin of this emission is not fully understood, but is commonly in observed in-both natural diamond and CVD-grown homoepitaxial single crystals and polycrystalline material[21,49,66]. It is known to be associated with dislocations and grain boundaries[67,68]. CL of other type IIa diamonds has shown that the dislocations themselves appear dark, indicating that they are non-radiative recombination centres, while surrounding material luminesces strongly[19], suggesting that a point defect atmosphere around dislocations is responsible. Interestingly, although deformation is confined to the brown bands the band-A luminescence is in fact roughly 30% lower there. The difference may be related to dislocation density, but it seems more probable that the cause is the difference in dislocation microstructure (e.g. straight vs curved dislocations, or dislocations vs dislocation dipoles).

The HPHT treatment almost completely removes brown colouration but the effect on physical microstructure is subtle at the length scales examined here. The natural variation in dislocation density and orientation from place to place effectively obscures any change that could be a result of the 2000 °C treatment. As seen in Fig. 13b the applied temperature is insufficient to produce annihilation of many dislocation dipoles, although it may be the case that dipoles with the narrowest spacings have annihilated. Certainly, the lack of any gross change in dislocation microstructure indicates that HPHT treatment mainly affects point defects, and the significant reduction in hydrostatic stress levels measured by the Raman line indicates that many point defects have been reincorporated into the lattice. In PL the strong line at 535.9 nm and the weak lines at 406, 491 and 423 nm are completely removed as are the equivalent lines in the CL spectra, indicating these point defect complexes are broken up by the anneal. The H3 and N3 lines also decrease in intensity by roughly 75%, when comparing their intensity to the first order Raman line, although the relative difference between brown and colourless bands does not change significantly. Since HPHT treatment is unlikely to change nitrogen content, it is plausible that this reduction must be the detachment of vacancies from these complexes and this agrees with the removal of vacancy clusters responsible for brown colouration[10]. These point defects presumably incorporate into the bulk of the crystal by mutual annihilation with interstitials or collapse into dislocation loops[17,69]. In CL, although the relative intensities of the N3 and band-A luminescence remain unchanged, the difference between the brown and colourless band-A intensities is greatly reduced from 30% to 10%, which probably indicates some change in dislocation microstructure at a finer scale than that examined here.

5. Conclusion

Correlative microscopy and spectroscopy has been used to image the point defect distributions and dislocation microstructures in a “zebra” diamond containing both brown and colourless bands. Large numbers of dislocation dipoles are observed in the brown bands, indicative of glide and interaction with forest dislocations during plastic deformation and the generation of intrinsic point defects. Raman maps show brown bands are under compressive stress, while colourless material is in tension. Dislocations in colourless material are curved and tangled and the difference in microstructure correlates with an increase in Band A emission in CL spectroscopy. The vacancies generated during plastic deformation agglomerate into clusters responsible for the colouration and can also be trapped at nitrogen defect complexes, such as the H3 defect found in larger concentrations in the brown bands. Weak lines at 406.3 nm and 491.3 nm are observed in brown bands of the untreated sample, matching those previously observed in other plastically deformed diamonds[2,63–65]. The defect responsible for these lines is unknown. The intensity of the defect line at 535.9 nm is strongly correlated to brown bands, to which we attribute plastic deformation forming an interstitial-type defect. After heat treatment three effects are primarily observed; the brown colouration reduces, these three PL lines are annealed out, and internal stresses reduce.

Acknowledgements

The authors would like to acknowledge Hugh Leach and John Freeth (De Beers Group IGNITE™), and Jon Newland (Element Six Ltd) for sample preparation. FHJL acknowledges the EPSRC Centre for Doctoral Training in Diamond Science and Technology (EP/L15315/1) and De Beers Group IGNITE™ for funding and loan of natural diamond samples. We thank Warwick Microscopy RTP and Warwick Spectroscopy RTP for the use of microscopes. The dataset relating to this publication can be found at: https://wrap.warwick.ac.uk/150606

References

[1] J.E. Shigley, E. Fritsch, A notable red-brown diamond, J. Gemmol. 23 (1993) 259–266.

[2] E. Gaillou, J.E. Post, N.D. Bassim, A.M. Zaitsev, T. Rose, M.D. Fries, R.M. Stroud, A. Steele, J.E. Butler, Spectroscopic and microscopic characterizations of color lamellae in natural pink diamonds, Diam. Relat. Mater. 19 (2010) 1207–1220. https://doi.org/10.1016/j.diamond.2010.06.015.

[3] B. Deljanin, D. Simic, A.M. Zaitsev, J. Chapman, I. Dobrinets, A. Widemann, N. Del Re, T. Middleton, E. Deljanin, A. De Stefano, Characterization of pink diamonds of different origin: Natural (Argyle, non-Argyle), irradiated and annealed, treated with multi-process, coated and synthetic, Diam. Relat. Mater. 17 (2008) 1169–1178. https://doi.org/10.1016/j.diamond.2008.03.014.

[4] I.A. Dobrinets, V.G. Vins, A.M. Zaitsev, HPHT-Treated Diamonds, 1st ed., Springer-Verlag Berlin Heidelberg, 2013. https://doi.org/10.1007/978-3-642-37490-6.

[5] S. Eaton-Magaña, T. Ardon, K.V. Smit, C.M. Breeding, J.E. Shigley, Natural-Color Pink, Purple, Red, and Brown Diamonds: Band of Many Colors, Gems Gemol. 54 (2017) 352–377.

[6] S. Eaton-Magaña, G. McElhenny, C.M. Breeding, T. Ardon, Comparison of gemological and spectroscopic features in type IIa and Ia natural pink diamonds, Diam. Relat. Mater. 105 (2020) 107784. https://doi.org/10.1016/j.diamond.2020.107784.

[7] M. Niewczas, Intermittent plastic flow of single crystals: Central problems in plasticity: A review, Mater. Sci. Technol. (United Kingdom). 30 (2014) 739–757. https://doi.org/10.1179/1743284713Y.0000000492.

[8] D. Howell, S. Piazolo, D.P. Dobson, I.G. Wood, A.P. Jones, N. Walte, D.J. Frost, D. Fisher, W.L. Griffin, Quantitative characterization of plastic deformation of single diamond crystals:

A high pressure high temperature (HPHT) experimental deformation study combined with electron backscatter diffraction (EBSD), Diam. Relat. Mater. 30 (2012) 20–30. https://doi.org/10.1016/j.diamond.2012.09.003.
[9] D. Howell, D. Fisher, S. Piazolo, W.L. Grifin, S.J. Sibley, Pink color in Type I diamonds : Is deformation twinning the cause?, Am. Mineral. 100 (2015) 1518–1527.
[10] D. Fisher, Brown diamonds and high pressure high temperature treatment, Lithos. 112 (2009) 619–624. https://doi.org/10.1016/j.lithos.2009.03.005.
[11] R.C. DeVries, Plastic deformation and "work-hardening" of diamond, Mater. Res. Bull. 10 (1975) 1193–1199. https://doi.org/10.1016/0025-5408(75)90026-4.
[12] E.J. Brookes, P. Greenwood, G. Xing, The plastic deformation and strain-induced fracture of natural and synthetic diamond, Diam. Relat. Mater. 8 (1999) 1536–1539.
[13] E.M. Smith, H.H. Helmstaedt, R.L. Flemming, Survival of the brown color in diamond during storage in the subcontinental lithospheric mantle, Can. Mineral. 48 (2010) 571–582. https://doi.org/10.3749/canmin.48.3.571.
[14] T. Stachel, J.W. Harris, The origin of cratonic diamonds - Constraints from mineral inclusions, Ore Geol. Rev. 34 (2008) 5–32. https://doi.org/10.1016/j.oregeorev.2007.05.002.
[15] M. Schoor, J.C. Boulliard, E. Gaillou, O. Hardouin Duparc, I. Estève, B. Baptiste, B. Rondeau, E. Fritsch, Plastic deformation in natural diamonds: Rose channels associated to mechanical twinning, Diam. Relat. Mater. 66 (2016) 102–106. https://doi.org/10.1016/j.diamond.2016.04.004.
[16] N. Hansen, C.Y. Barlow, Plastic Deformation of Metals and Alloys, Fifth Edit, Elsevier, 2014. https://doi.org/10.1016/B978-0-444-53770-6.00017-4.
[17] B. Willems, P.M. Martineau, D. Fisher, J. Van Royen, G. Van Tendeloo, Dislocation distributions in brown diamond, Phys. Status Solidi Appl. Mater. Sci. 203 (2006) 3076–3080. https://doi.org/10.1002/pssa.200671129.
[18] J.P. Hirth, On dislocation interactions in the fcc lattice, J. Appl. Phys. 32 (1961) 700–706. https://doi.org/10.1063/1.1736074.
[19] F.H.J. Laidlaw, R. Beanland, D. Fisher, P.L. Diggle, Point defects and interstitial climb of 90° partial dislocations in brown type IIa natural diamond, Acta Mater. 201 (2020) 494–503. https://doi.org/10.1016/j.actamat.2020.10.033.
[20] A.T. Collins, A spectroscopic survey of naturally-occurring vacancy-related colour centres in diamond, J. Phys. D. Appl. Phys. 15 (1982) 1431–1438. https://doi.org/10.1088/0022-3727/15/8/014.
[21] P.L. Hanley, I. Kiflawi, A.R. Lang, On topographically identifiable sources of cathodoluminescence in natural diamonds, Philos. Trans. R. Soc. London. Ser. A, Math. Phys. Sci. 284 (1977) 329–368.
[22] S.T. Davey, T. Evans, S.H. Robertson, An investigation of plastic deformation in sintered diamond compacts using photoluminescence spectroscopy, J. Mater. Sci. Lett. 3 (1984) 1090–1092. https://doi.org/10.1007/BF00719773.
[23] R.M. Mineeva, S.V. Titkov, A.V. Speransky, Structural defects in natural plastically deformed diamonds: Evidence from EPR spectroscopy, Geol. Ore Depos. 51 (2009) 233–242. https://doi.org/10.1134/S1075701509030052.
[24] L. Massi, E. Fritsch, A.T. Collins, T. Hainschwang, F. Notari, The "amber centres" and their relation to the brown colour in diamond, Diam. Relat. Mater. 14 (2005) 1623–1629. https://doi.org/10.1016/j.diamond.2005.05.003.
[25] J.M. Mäki, F. Tuomisto, C.J. Kelly, D. Fisher, P.M. Martineau, Properties of optically active vacancy clusters in type IIa diamond, J. Phys. Condens. Matter. 21 (2009). https://doi.org/10.1088/0953-8984/21/36/364216.
[26] R. Jones, Dislocations, vacancies and the brown colour of CVD and natural diamond, Diam. Relat. Mater. 18 (2009) 820–826. https://doi.org/10.1016/j.diamond.2008.11.027.
[27] U. Bangert, R. Barnes, M.H. Gass, A.L. Bleloch, I.S. Godfrey, Vacancy clusters, dislocations and brown colouration in diamond, J. Phys. Condens. Matter. 21 (2009). https://doi.org/10.1088/0953-8984/21/36/364208.
[28] V. Avalos, S. Dannefaer, Vacancy-type defects in brown diamonds investigated by positron annihilation, Phys. B Condens. Matter. 340–342 (2003) 76–79.

https://doi.org/10.1016/j.physb.2003.09.006.
[29] L.S. Hounsome, R. Jones, P.M. Martineau, M.J. Shaw, P.R. Briddon, S. Öberg, A.T. Blumenau, N. Fujita, Optical properties of vacancy related defects in diamond, Phys. Status Solidi Appl. Mater. Sci. 202 (2005) 2182–2187. https://doi.org/10.1002/pssa.200561914.
[30] L.S. Hounsome, R. Jones, P.M. Martineau, D. Fisher, M.J. Shaw, P.R. Briddon, S. Öberg, Role of extended defects in brown colouration of diamond, Phys. Status Solidi Curr. Top. Solid State Phys. 4 (2007) 2950–2957. https://doi.org/10.1002/pssc.200675443.
[31] J.M. Mäki, T. Kuittinen, E. Korhonen, F. Tuomisto, Positron lifetime spectroscopy with optical excitation: A case study of natural diamond, New J. Phys. 14 (2012). https://doi.org/10.1088/1367-2630/14/3/035023.
[32] N. Fujita, R. Jones, S. Öberg, P.R. Briddon, Large spherical vacancy clusters in diamond - Origin of the brown colouration?, Diam. Relat. Mater. 18 (2009) 843–845. https://doi.org/10.1016/j.diamond.2008.10.061.
[33] L.S. Hounsome, R. Jones, P.M. Martineau, D. Fisher, M.J. Shaw, P.R. Briddon, S. Öberg, Origin of brown coloration in diamond, Phys. Rev. B - Condens. Matter Mater. Phys. 73 (2006) 1–8. https://doi.org/10.1103/PhysRevB.73.125203.
[34] P.T. Heald, The preferential trapping of interstitials at dislocations II. The effect of competition between neighbouring dislocations, Philos. Mag. 34 (1976) 647–652. https://doi.org/10.1080/14786437608223802.
[35] G. Davies, M.H. Nazare, M.F. Hamer, H3 (2.463 eV) Vibronic Band in diamond: Uniaxial Stress Effects and the Breakdown of Mirror Symmetry., Proc R Soc London Ser A. 351 (1976) 245–265. https://doi.org/10.1098/rspa.1976.0140.
[36] K.S. Byrne, J.D. Anstie, J.G. Chapman, A.N. Luiten, Optically reversible photochromism in natural pink diamond, Diam. Relat. Mater. 30 (2012) 31–36. https://doi.org/10.1016/j.diamond.2012.09.005.
[37] K.S. Byrne, J.G. Chapman, A.N. Luiten, Erratum: Photochromic charge transfer processes in natural pink and brown diamonds (Journal of Physics Condensed Matter (2014) 26 (035501)), J. Phys. Condens. Matter. 26 (2014). https://doi.org/10.1088/0953-8984/26/23/239502.
[38] D. Schiferl, M. Nicol, J.M. Zaug, S.K. Sharma, T.F. Cooney, S.Y. Wang, T.R. Anthony, J.F. Fleischer, The diamond 13C/12C isotope Raman pressure sensor system for high-temperature/pressure diamond-anvil cells with reactive samples, J. Appl. Phys. 82 (1997) 3256–3265. https://doi.org/10.1063/1.366268.
[39] J.M. Boteler, Y.M. Gupta, Shock Induced Splitting of the Triply Degenerate Raman Line in Diamond, Phys. Rev. Lett. 71 (1993) 3497–3500.
[40] S. Amelinckx, Dislocations in Solids Vol. 2 Chapter 6 (edited by F.R.N Nabarro), North-Holland Publishing Co., Amsterdam, 1979.
[41] F. Seitz, On the generation of vacancies by moving dislocations, Adv. Phys. 1 (1952) 43–90. https://doi.org/10.1080/00018735200101161.
[42] H. Suzuki, A Mechanism of Formation of Dislocation Dipoles in FCC Crystals, J. Phys. Soc. Japan. 20 (1965) 1639–1647.
[43] A. Seeger, CXXXII. The generation of lattice defects by moving dislocations, and its application to the temperature dependence of the flow-stress of F.C.C. crystals, London, Edinburgh, Dublin Philos. Mag. J. Sci. 46 (1955) 1194–1217. https://doi.org/10.1080/14786441108520632.
[44] G.F. Vander Voort, ASM Handbook Volume 9: Metallography and Microstructures, ASM International, 2004.
[45] L.M. Brown, Constant intermittent flow of dislocations: Central problems in plasticity, Mater. Sci. Technol. (United Kingdom). 28 (2012) 1209–1232. https://doi.org/10.1179/174328412X13409726212768.
[46] A. Mussi, D. Eyidi, A. Shiryaev, J. Rabier, TEM observations of dislocations in plastically deformed diamond, Phys. Status Solidi Appl. Mater. Sci. 210 (2013) 191–194. https://doi.org/10.1002/pssa.201200483.
[47] M.E. Newton, B.A. Campbell, D.J. Twitchen, J.M. Baker, T.R. Anthony, Recombination-enhanced diffusion of self-interstitial atoms and vacancy-interstitial recombination in diamond, Diam. Relat. Mater. 11 (2002) 618–622. https://doi.org/10.1016/S0925-9635(01)00623-9.

[48] M.W. Dale, Colour centres on demand in diamond, University of Warwick, 2015. http://wrap.warwick.ac.uk/80044/.
[49] A.M. Zaitsev, Optical Properties of Diamond A Data Handbook, 1st ed., Springer-Verlag Berlin Heidelberg, 2001. https://doi.org/https://doi.org/10.1007/978-3-662-04548-0.
[50] A.D. Brailsford, R. Bullough, The rate theory of swelling due to void growth in irradiated metals, J. Nucl. Mater. 44 (1972) 121–135. https://doi.org/10.1016/0022-3115(72)90091-8.
[51] H. Wiedersich, On the theory of void formation during irradiation, Radiat. Eff. 12 (1972) 111–125. https://doi.org/10.1080/00337577208231128.
[52] S. Eaton-magaña, C.M. Breeding, A.C. Palke, A. Homkrajae, Z. Sun, G. McElhenny, Raman and photoluminescence mapping of gem materials, Minerals. 11 (2021) 1–32. https://doi.org/10.3390/min11020177.
[53] S. Eaton-Magaña, C.M. Breeding, An Introduction to Photluminescence Spectroscopy for Diamond and Its Applications in Gemology, Gems Gemol. 52 (2016) 2–17.
[54] K.S. Byrne, J.D. Anstie, J. Chapman, A.N. Luiten, Infrared microspectroscopy of natural Argyle pink diamond, Diam. Relat. Mater. 23 (2012) 125–129. https://doi.org/10.1016/j.diamond.2012.01.032.
[55] T. Gu, W. Wang, Optical defects in milky type IaB diamonds, Diam. Relat. Mater. 89 (2018) 322–329. https://doi.org/10.1016/j.diamond.2018.09.010.
[56] S. Eaton-Magaña, T. Ardon, A.M. Zaitsev, LPHT annealing of brown-to-yellow type Ia diamonds, Diam. Relat. Mater. 77 (2017) 159–170. https://doi.org/10.1016/j.diamond.2017.06.008.
[57] A.T. Collins, A. Connor, C. Ly, A. Shareef, P.M. Spear, High-temperature annealing of optical centers in type-I diamond, J. Appl. Phys. 97 (2005). https://doi.org/10.1063/1.1866501.
[58] R. Jones, J.P. Goss, H. Pinto, D.W. Palmer, Diffusion of nitrogen in diamond and the formation of A-centres, Diam. Relat. Mater. 53 (2015) 35–39. https://doi.org/10.1016/j.diamond.2015.01.002.
[59] J.W. Steeds, T.J. Davis, S.J. Charles, J.M. Hayes, J.E. Butler, 3H luminescence in electron-irradiated diamond samples and its relationship to self-interstitials, Diam. Relat. Mater. 8 (1999) 1847–1852. https://doi.org/10.1016/S0925-9635(99)00144-2.
[60] K. Iakoubovskii, I. Kiflawi, K. Johnston, A. Collins, G. Davies, A. Stesmans, Annealing of vacancies and interstitials in diamond, Phys. B Condens. Matter. 340–342 (2003) 67–75. https://doi.org/10.1016/j.physb.2003.09.005.
[61] D. Fisher, R.A. Spits, Spectroscopic Evidence of Ge Pol HPHT-Treated Natural Type IIa Diamonds, Gems Gemol. 36 (2000) 42–49.
[62] A. Shareef, A.T. Collins, D. Fisher, The 536 and 576 nm centres in diamond, in: 56th Diam. Conf. Abstr., 2005.
[63] V.A. Nadolinny, O.P. Yurjeva, N.P. Pokhilenko, EPR and luminescence data on the nitrogen aggregation in diamonds from Snap Lake dyke system, Lithos. 112 (2009) 865–869. https://doi.org/10.1016/j.lithos.2009.05.045.
[64] R.J. Graham, P.R. Buseck, Cathodoluminescence of brown diamonds as observed by transmission electron microscopy, Philos. Mag. B Phys. Condens. Matter; Stat. Mech. Electron. Opt. Magn. Prop. 70 (1994) 1177–1185. https://doi.org/10.1080/01418639408240282.
[65] A.T. Collins, G.S. Woods, Cathodoluminescence from “giant” platelets, and of the 2.526 eV vibronic system, in type Ia diamonds, Philos. Mag. B Phys. Condens. Matter; Stat. Mech. Electron. Opt. Magn. Prop. 45 (1982) 385–397. https://doi.org/10.1080/01418638208227446.
[66] S.J. Pennycook, L.M. Brown, A.J. Craven, Observation of cathodoluminescence at single dislocations by STEM, Philos. Mag. A Phys. Condens. Matter, Struct. Defects Mech. Prop. 41 (1980) 589–600. https://doi.org/10.1080/01418618008239335.
[67] D. Takeuchi, H. Watanabe, H. Sawada, S. Yamanaka, H. Ichinose, T. Sekiguchi, H. Okushi, Origin of band-A emission in homoepitaxial diamond films, Diam. Relat. Mater. 10 (2001) 526–530. https://doi.org/10.1016/S0925-9635(00)00491-X.
[68] D. Takeuchi, H. Watanabe, S. Yamanaka, H. Okushi, H. Sawada, H. Ichinose, T. Sekiguchi, K. Kajimura, Origin of band-A emission in diamond thin films, Phys. Rev. B - Condens. Matter Mater. Phys. 63 (2001) 1–7. https://doi.org/10.1103/PhysRevB.63.245328.

[69] B. Willems, Structural Defects and Colour-Treated Diamond: A Transmission Electron Microscopy Study, Antwerp, 2006.